Thermal Simulations for the Target Station at FAIR

by

Yahia Mostafa

Supervised by: Dr. Catherine Rigollet

Second examiner: Dr. Julia Even

A thesis submitted in partial fulfilment of the degree of Bachelor of Physics

at the

Faculty of Sciences and Engineering

KVI-CART

July 2018

Declaration of Authorship

I, Yahia Yasser Mostafa, declare that this thesis titled, 'Thermal Simulations for the Target Station at FAIR' and the work presented in it are my own. I confirm that:

- This work was done wholly while in study at this University.
- Where any part of this thesis has previously been submitted for a degree or any other qualification or course at this University or any other institution, this has been clearly stated.
- Where I have consulted the published work of others, this is always clearly attributed.
- Where I have quoted from the work of others, the source is always given. With the exception of such quotations, this thesis is entirely my own work.
- I have acknowledged all main sources of help.
- Where the thesis is based on work done by myself jointly with others, I have made clear exactly what was done by others and what I have contributed myself.

Signed:

Date: 06/07/2018

Abstract

Recent technological developments have allowed for the creation and maintenance of high energy ion beams. At FAIR in Germany, to create exotic nuclei, high intensity ion beams are set to collide with a rotating graphite target wheel. The wheel is driven by a motor, placed within a target station hosting beam diagnostic detectors and a collimator. The beam-material interactions generate 4 kW of thermal power in the wheel. To ensure normal operation of the motor and detectors in the target station, a cooling system is implemented. Finite element method thermal and flow calculations have been executed to determine the temperatures of the motor and detectors and to assess the efficiency of the cooling system. The cooled motor system is found to not exceed $50°C$ and the cooling system is found to extract 47% of the deposited power.

Acknowledgements

I would like to thank Dr. C. Rigollet for the offering of this project, accomplished supervision and guidance, extended help, and inclusion in the Nuclear & Hadron Physics research unit. I would like to offer my special thanks to Dr. J. Even for the help and guidance with the current work. I would like to express gratitude to Prof. dr. N. Kalantar for the advice and direction given throughout my time at KVI-CART.

I would like to further extend thanks to Ir. H. Smit and B Eng. M.F. Lindemulder for sharing their work, as CAD drawings, and their help on the operation of the simulation software. My special thanks are extended to the staff of the FAIR unit, nuclear and hadron group and the KVI-CART staff at the University of Groningen.

Contents

Chapter 1

Introduction

Throughout the last century there has been increasing scientific interest in the structure of matter, the fundamental forces and interactions of nature. This interest has lead to the development and production of large scale scientific experiments, targeted at investigating the building blocks of physical structures. A standard method of probing fundamental particles is through controlled particle-particle collisions. This is the method mainly used at large particle accelerators such as GSI (Helmholtz Centre for Heavy Ion Research) located in Darmstadt, Germany.

Particle-particle collisions in large accelerators provide valuable insight into fundamental particle and nuclear physics. Collisions are employed to probe the standard model and investigate exotic states of matter and nuclear forces. Essentially, particle collisions can occur between two travelling beams of particles or between a travelling beam and a stationary target with respect to the laboratory.

The purpose of the current work is to investigate the thermal effects of incident ion beams on a stationary target at GSI/FAIR. While the interactions of such high energy particles with the target produce desired rare products and expand our knowledge, they result in a large amount of energy deposited in the target material. This dissipation energy lost by the particle beam is manifested as heat and increases the temperature of the target and the surrounding environment considerably. The specific objective of this study is to examine the effects of the incident heat load by executing thermal simulations of the target and its surroundings to ensure safe operation.

This thesis is divided into six chapters as follows. The first and current chapter is an introduction to the work which lays down the fundamental concepts and motivation to conduct this research. The second chapter covers the theoretical models used throughout, with an explanation and reasoning behind the inclusion of specific physical models as opposed to valid alternatives. The third chapter is specific to the thesis, giving an overview of the framework, computational models used and the implementation of the relevant physical models into simulations. Chapter 4 presents the results of the studies discussed. Accordingly, chapter 5 is a discussion on the presented results and analyses. The final chapter concludes the thesis, relating results to the initial motivation of the study, as well as providing suggestions for future research.

1.1 GSI

The GSI Helmholtz Centre for Heavy Ion Research in Darmstadt, Germany has been a leading facility in the research in particle and nuclear physics for several decades. This has been demonstrated by many experimental discoveries including six new chemical elements and the development of ion beam cancer treatment. In the coming years, GSI is focused on the construction and operation of the new international accelerator Facility for Anti-proton and Ion Research (FAIR). This facility is focused on investigations into the structure of matter using radioactive ion beams. There are four scientific collaborations of FAIR targeting different aspects of the investigation into the physics of the fundamental particles and nuclei.

Atomic, Plasma Physics and Applications (APPA) is one of the four collaborations and focuses on plasma and high energy density physics as well as the research and development of material hardened to extreme conditions [1]. As stated in the GSI literature, the major focus point of the APPA collaboration is to examine how materials and cells react to incident radiation [2].

The Compressed Baryonic Matter (CBM) explores the quantum chromo-dynamical interactions at high baryon densities. The CBM collaboration also studies equations of states of nuclear matter at densities equivalent to what is found in neutron stars [3].

The anti-Proton ANnihilation at DArmstadt (PANDA) uses proton and anti-proton beams to study strong interaction physics and exotic states. This collaboration is directed at studying the charmonium particle interactions and spectroscopy, as well as studying hypernuclei production and decay [4].

Nuclear Structure, Astrophysics and Reactions (NUSTAR) is the fourth scientific pillar of FAIR, operating with beams of radioactive ions to study the limits of nuclear stability and shell structure possible changes, amongst other topics. The NUSTAR collaboration is the parent collaboration for the study of this thesis. Central to this collaboration is the Superconducting FRagment Separator (SFRS) which produces, identifies and separates radioactive species.

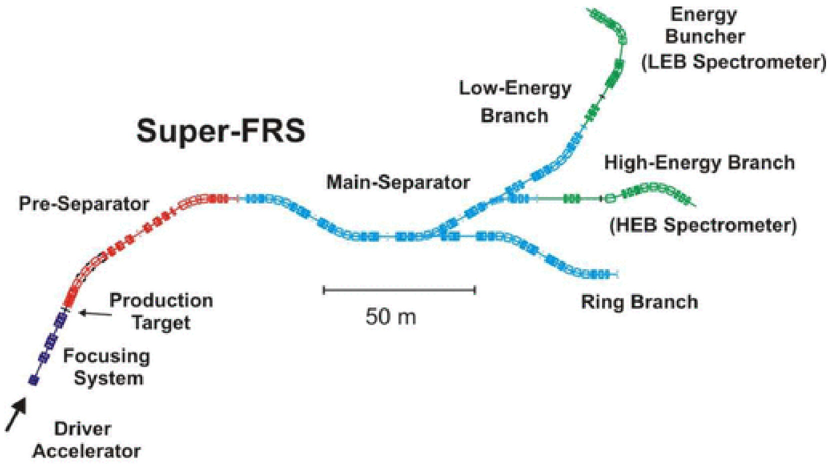

FIGURE 1.1: Schematic overview of the SFRS detailing the location of the production target.

1.2 Superconducting FRagment Separator (SFRS)

The SFRS is a superconducting projectile fragment separator currently being developed as a successor to the existing FRS [5]. The apparatus is a magnetic spectrometer handling beams of all elements from hydrogen through uranium. The separator operates under intensities up to 10^{12} ions per second with maximum energies of 1.5 GeV/u [6]. The SFRS is sequenced before 3 major experimental branches and is divided into a pre-separator and a main-separator. The pre-separator consists of a focusing system and a target station in which the production target wheel is placed. Figure 1.1 shows the schematic overview of the facility and the location of the production target. The current thesis includes analyses on the thermal simulations of the production target station.

1.2.1 Physics Goals

The NUSTAR collaboration operating the SFRS is aimed at understanding and discovering new physical phenomena related to nuclear physics. There are many specific physics goals to the collaboration, for a complete summary please refer to reference [7]. Here, a brief overview of the experimental ambitions to be achieved by the SFRS is given.

Various experiments utilise the SFRS to produce neutron-rich isotopes with the goals of defining and reaching the neutron drip line and ultimately to study of r-process nucleosynthesis [7]. This search will focus on regions of masses between Sn and U, where the nuclei in question will become completely ionised and identified with high accuracy. Furthermore, studies into the strong force interactions within nuclei will be of interest.

In these studies, the production and decay of hyper-nuclei will be analysed to understand the interactions between particles occurring within hyper-nuclei and consequently, exotic nuclei in general [6].

1.2.2 Target Station

As described earlier, the target station is the main interest of the current study and is placed at the beginning of the pre-separator at the SFRS. The target station hosts a graphite target wheel and several beam diagnostic and modification devices. These include a collimator and three plugs containing several detectors each. The three detector ladders shown in figure 1.2 in green carry three detectors each: a diamond detector, a SEETRAM detector and an SEM grid detector all designed for beam analysis. As shown in figure 1.2, the target wheel is placed between the detectors and the collimator, with respect to the beam direction.

1.2.3 Target Wheel

The primary component of the target station at SFRS is the target itself. Since there is a large incident amount of energy on the target, a design choice has been made to maximise the interaction volume by introducing a rotating wheel as a target as opposed to a stationary block. By maximising the volume as such, ion beam heating has less of an effect on the material properties and the lifetime of the wheel increases. Additionally, with such design an effective cooling system can be implemented. The target wheel is placed in the fourth plug from the beam direction as shown in Figure 1.2.

The target wheel's material is chosen to be graphite. The wheel is manufactured by the SGL Group (fine grain Sigrafine® R6650). The material properties of the product are well known, except for emissivity which is to be estimated (Refer to section 2.2.2.1). There exists a prototype of the target wheel, however, it is not available for the current study.

The target wheel is 45 cm in diameter with its geometry is divided into 5 steps to provide varying thicknesses for the relevant experiments to be conducted. The 5 steps are each 16mm wide giving rise to thicknesses of 5.4, 13.5, 21.6, 32.4 and 43.2 mm corresponding to 1, 2.5, 4, 6, and 8 gcm^{-2}, respectively [8]. A schematic of the target wheel is shown in Figure 1.3.

The wheel rotation is induced by a stepper motor with 200 steps per rotation. The motor is of the company Phytron®, designed to sustain ultra-high vacuum and high short term winding temperatures. The particular product chosen is the VSH 120 stepper

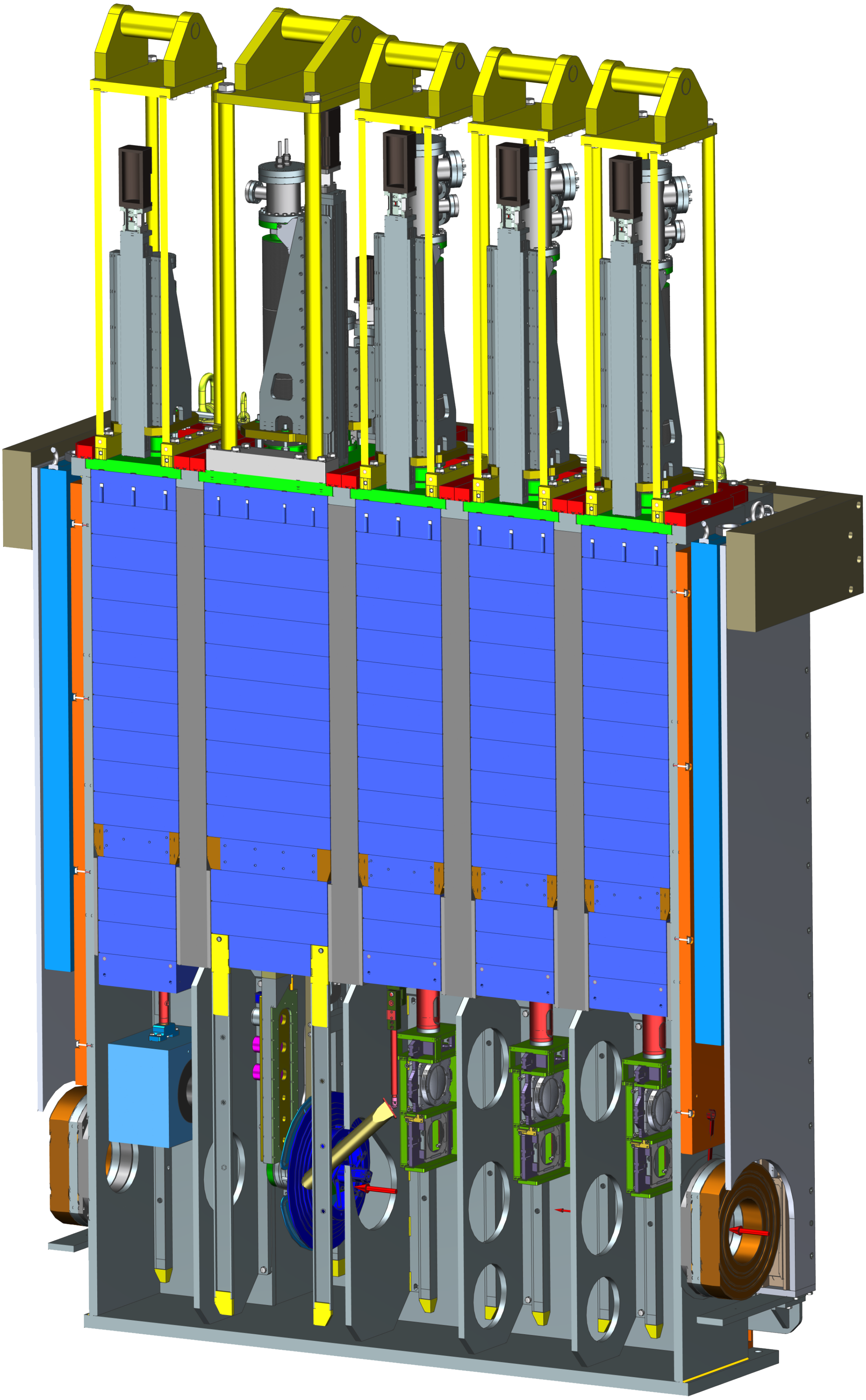

Figure 1.2: Cut-through view of the target station at the SFRS facility. From left to right: the collimator plug, target plug and 3 detector plugs

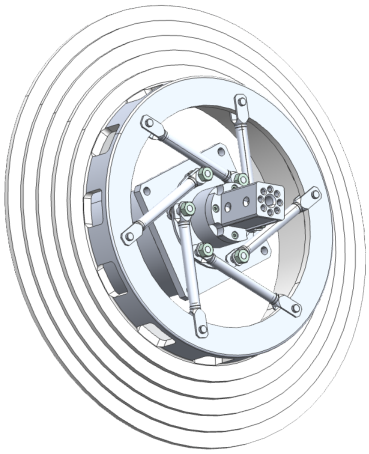

FIGURE 1.3: The target wheel isolated from the target station

motor. The wheel is attached to the motor through six spokes. The spokes' material is chosen to be a nickel-chromium alloy, INCONEL® alloy 600, specifically designed to withstand high temperature conditions.

1.2.4 Cooling System

A water cooling system for the target chamber is designed and modelled by B. Eng. M.F. Lindemulder at KVI-CART, Groningen. The system consists of three plates: front, back, and motor cooling plates as shown in figure 1.4. The motor plate outlet is connected to the back plate such that both plates are cooled through the same water conveyance system.

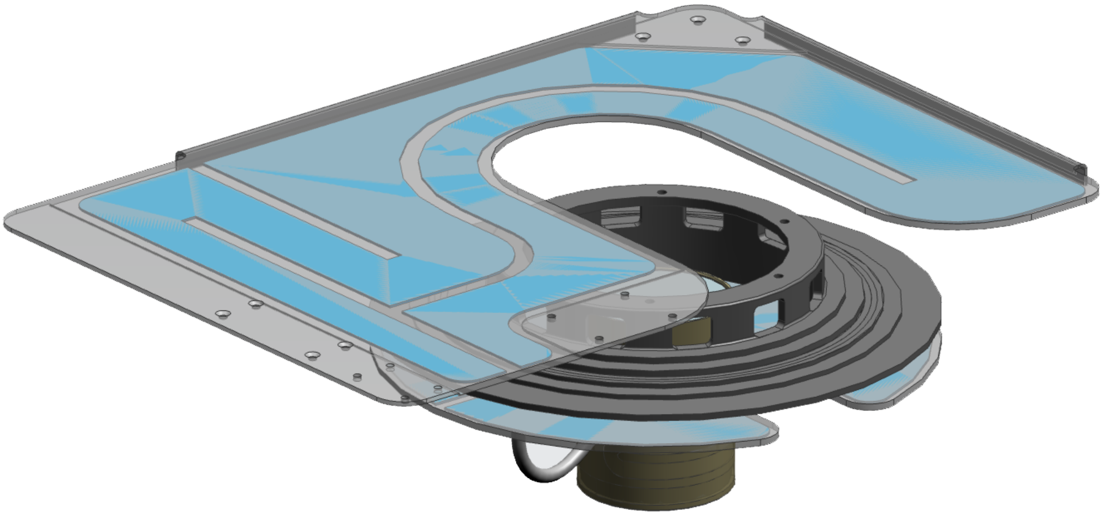

FIGURE 1.4: Target wheel and motor with the cooling system. The motor spokes are excluded from the figure.

Chapter 2

Theoretical Background

This chapter is aimed at introducing the theoretical physical models used in the simulations and analyses which follow. The mathematical framework for the physical models is explained and the motivation for the inclusion of such models is presented. First, an explanation of the physics behind ion beam irradiation is given, which is the primary heating mechanism for the target wheel studied in this thesis. Subsequently, physical models for heat transfer and fluid flow mechanisms are explained.

Heat transfer between objects can occur through three different mechanisms: conduction, convection and radiation. Conduction occurs between media in direct contact with each other and is governed by the thermo-mechanical collisions of the particles in the medium. Convection is the heat flow through the mass movement of the constituent particles. Since convection requires particle mobilisation, it occurs in fluids only. Additionally, while conduction and convection require a medium, radiation does not. Radiation is the process of heat transfer by emission and absorption of electromagnetic waves. The energy of the electromagnetic waves is absorbed by an object and adds to its thermal energy.

The physical models discussed here are automatically present as a feature of the Siemens NX 10.0 software used to execute the simulations or are incorporated into the simulations by the author. When the latter case is true, this will be indicated.

2.1 Ion Beam−Material Interaction

Beam-material interactions is a vital topic to be considered as energies of particle beams in accelerators increase. This subject targets the study of the behaviour of the particle beam at incidence with the accelerator material, detectors and targets [9].

The target station and consequently the target wheel expects to receive a variety of input ion beam at diverse energies. The varying incoming beam energies result in different deposited energies in the target wheel. In the current analysis, beams are considered to have 1 A GeV energy at 10^{12} ions/pulse. Typical beam parameters and corresponding energies are shown in Table 2.1. The beam spot for the relevant calculations is assumed to have a Gaussian shape with standard deviations 3mm radially [8].

Table 2.1: Typical beam parameters for selected ions at 1 A GeV energy with 10^{12} ions/pulse [8]

Beam	Total Beam Energy [kJ]	Graphite Target Thickness [g/cm^2]	Deposited Energy [kJ]	Specific Energy[kJ/g]
^{40}Ar	6.4	8.0	0.83	0.83
^{136}Xe	21.8	6.0	6.0	7.9
^{238}U	38.1	4.0	12.0	24

For the Super-FRS, the total beam power does not exceed 38 kW, resulting in a maximum deposited power of 12k kW on the target wheel [8]. Of those 12 kW, the maximum total thermal power is 4 kW. This is as per the specifications provided by the GSI contact person for this project.

2.2 Heat Transfer

Heat transfer occurs in three different ways, of which, only conduction and radiation are discussed here. Convection is deemed not relevant to the study of this thesis since the system under study is placed in high vacuum, eliminating the presence of convection fluid surrounding the system. Additionally, fluids present in the cooling system are only studied under the flow conditions. In this section, basic principles behind conduction and radiation are presented as fundamental concepts for the analyses of the current study.

2.2.1 Conduction

The transfer of kinetic energy through molecular and atomic collisions over a distance is what is known macroscopically as heat conduction. Consider two object at temperature T_1 and T_2 at contact with one another through a surface of area A and a connection length l. The heat transfer rate, heat flow, is given by:

$$\frac{\Delta Q}{\Delta t} = kA\frac{(T_1 - T_2)}{l}$$

Here, k is a constant of proportionality known as thermal conductivity. Materials with large k values are said to be good thermal conductors and conversely, for small k, the material is regarded as an insulator. In the defining limit, as the length l goes infinitesimally small, the heat flow between two adjacent points becomes:

$$\frac{dQ}{dt} = -kA\frac{dT}{dx}$$

Such that the heat flow is directionally opposite to the temperature gradient $\frac{dT}{dx}$. The complete heat transfer in a 2 dimensional solid is governed by the Laplacian equation:

$$k(\frac{\partial^2 T}{\partial x^2} + \frac{\partial^2 T}{\partial y^2}) = \rho C\frac{\partial T}{\partial t}$$

which is an extension of the equations described before. Here, ρ is the material density and C is the associated specific heat.

2.2.2 Radiation

Radiation heat transfer is the emission and absorption of thermal energy through electromagnetic waves. An object radiates discrete quanta of light, photons, at certain wavelengths depending on its temperature. The energy of a photon is given by:

$$E = h\gamma$$

where h is the Planck's constant and γ the frequency of the photon. To analyse the total radiation emitted by a body, it is sufficient to consider the photons radiated as a 'photon gas' carrying energy away from the body. Accordingly, through studying the quantum statistical dynamics of the gas, one can conclude the energy density per unit volume per wavelength as:

$$u_\lambda = \frac{8\pi hc\lambda^{-5}}{e^{\frac{hc}{\lambda kT}} - 1}$$

where k is the Boltzmann's constant and the temperature T is in Kelvins. Integrated over all emitted wavelengths, the total energy is given by Stefan-Boltzmann law:

$$E_b = \sigma T^4$$

Where σ is the Stefan-Boltzmann constant. E_b describes the energy transmitted by an ideal black-body radiator.

The rate at which an object loses energy through radiation is, therefore, a function of the fourth power of its temperature, T. Additionally, radiation to the environment increases with increasing surface area, A, of an object. However, different surfaces will emit different amounts of radiation depending on surface topology and material properties. This change in emission is characterised by a parameter known as the emissivity of an object, denoted as ϵ; it describes the effectiveness of a surface in emitting energy in the form of radiation. The characteristics of emissivity are the subject of the following subsection. In consideration of the aforementioned factors, the rate of energy loss in an object through thermal radiation is given by the Stefan-Boltzmann equation to be:

$$E = \frac{\Delta Q}{\Delta t} = \epsilon \sigma A T^4$$

Since an object not only radiates energy but absorbs energy through radiation, this is reflected in the total heat transfer by radiation. If an object with surface area A and emissivity ϵ at temperature T is placed in an environment of temperature T_0, the energy loss through radiation is given by the difference between radiated and absorbed energies as:

$$\frac{\Delta Q}{\Delta t} = \epsilon \sigma A (T^4 - T_0^4)$$

2.2.2.1 Emissivity (ϵ)

Not all materials and objects thermally radiate equally. In thermal analysis, emissivity is a dimensionless factor which determines the amount of energy lost through radiation. Emissivity is the ratio of the amount of radiation emitted by an object compared to an identical black body's radiation. The value of emissivity varies from 0 up to 1.

The emissivity of an object is highly dependent on the characteristics of the material, its surface and its temperature. Accordingly, minute changes in the surface roughness directly affect the value of the emissivity. Thus for time varying surface geometry, which is for example present through ion beam etching, the emissivity becomes time-dependent. Additionally, since the surface temperature affects the emissivity, there is further dependence of the value on the time evolution of the system. These complications are addressed in the current work, however, no experimental work has been conducted to determine the degrees of dependency. In such cases where the temperature or temporal dependencies are unknown, worst case scenarios are considered.

2.2.2.2 Grey Body View Factors

A Grey Body View Factor (GBVF) characterises the fraction of energy leaving a surface being absorbed by a secondary surface. For an object surrounded completely by another, the GBVF between the two objects is one. Let F_{12}=F_{21} be the fraction of energy exchange between surfaces 1 and 2. The net energy exchange, assuming the surfaces are black bodies is then:

$$Q_{1-2} = E_{b1}A_1F_{12} - E_{b2}A_2F_{21}$$

Where A indicate the area of the surface and E denotes total energy radiated, with respective subscripts. For the analysis of grey bodies, the emissivity factor is to be considered into the equation. By calculating the GBVFs of surfaces in the studied system, the radiation between the objects is determined.

2.3 Flow

Since one of the aims of the current thesis is to develop an adequate cooling system for the target wheel, fluid dynamics will be considered. The cooling mechanism employed at the target station is water cooling by the means of narrow water pipes in plates around the wheel and the motor. To assess the efficiency of the cooling system, the water's thermal and dynamical properties need to be carefully studied. This section will introduce basic principles in this domain which are used in all simulations concerning the cooling system.

2.3.0.1 Laminar Flow

Laminar flow is the linear motion of the fluid without perturbations within a container. Laminar flow exhibits a simple velocity profile such as shown in figure 2.1. Due to friction with the wall, the velocity of the fluid near the boundaries is lower than away from the wall. The velocity at which the fluid flows with no friction is called the free-stream velocity, u_∞, which occurs, for example, at the centre of a cylindrical pipe.

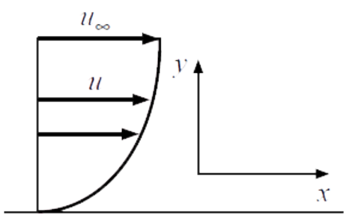

FIGURE 2.1: Velocity, u, profile of laminar flow near a boundary [10]

2.3.0.2 Turbulent flow

The turbulent flow of a fluid could be imagined as a linear transformation of a combination of small packets of fluid moving in all directions vigorously. The transition between laminar and turbulent flow occurs when

$$\frac{u_\infty x}{v} > 5 \times 10^5$$

where x is the distance from the initial inlet edge and v is the kinematic viscosity. This dimensionless ratio, $\frac{u_\infty x}{v}$, is also known as Reynolds number, Re. Although turbulent flow is characterised by $Re > 10^5$, depending on the geometry this limiting value might change. In the intermediate region between laminar flow and turbulent flow there is a transition phase such as shown in 2.2. In this transition region, small disturbances in the previously linear flow occur, eventually leading to turbulence.

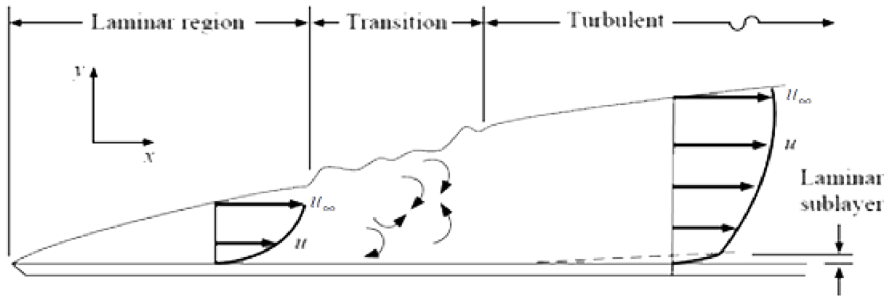

FIGURE 2.2: Different flow conditions and their corresponding velocity profiles [10]

Chapter 3

Finite Element Simulations

The Finite Element Method (FEM) is a computational numerical method employed in many engineering and physical analyses. The method depends mainly on dividing the volume in the analyses in many discrete sub-parts or elements. Through this discretisation, the mathematical models of the physics considered are transformed into numerical calculations. By dividing the volume, the analysis is then reduced to the boundary conditions at the confines of each element. As a result of this discretisation process, meshes of elements are produced and thus the process is referred to as meshing the volume. The program used to execute the simulations is Siemens NX 10.0 under the licence obtained by the University of Groningen.

This chapters begins by explaining the meshing mechanism in the FEM analyses. Subsequently, a description is given of the incorporated physical models for thermal, flow and mechanical studies. Finally, the solutions' criteria are constructed and an explanation is given of the solution types and their relevance to the physical scenario.

3.1 Meshing

This section is based on the work of J.P. Holman in 'Heat Transfer' [10]. The descriptions provided here are adaptations of the text and adjusted to the relevant analyses of the current study.

In the thermal analysis of solid bodies, the equation governing heat flow based on the descriptions given in chapter 2 can be written as:

$$k\left(\frac{\partial^2 T}{\partial x^2} + \frac{\partial^2 T}{\partial y^2}\right) = \rho C \frac{\partial T}{\partial t}$$

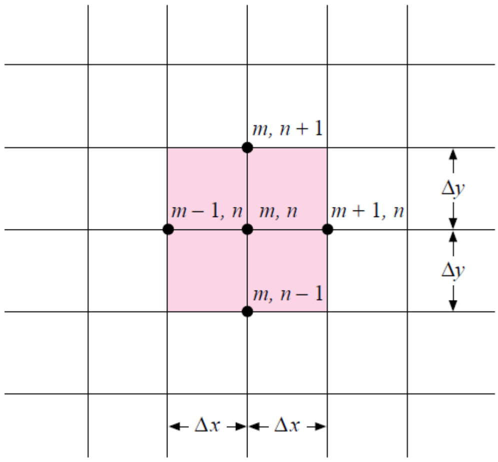

FIGURE 3.1: Two dimensional meshing mechanism for numerical solutions of heat flow [10]

It is our goal to simplify these continuous governing equations into simpler models of linear dependencies to achieve a numerical solution. As an example, assume a two dimensional geometry, where the area is divided or meshed into smaller areas of $\Delta x \times \Delta y$ as depicted in figure 3.1. The nodes of the elements are labelled with m in the x direction and n in the y direction. The continuous equations can now be discretised as such to achieve linear dependencies. Assuming time independent parameters, the partial derivatives can be approximated using the secant method to:

$$\frac{\partial^2 T}{\partial x^2} \approx \frac{1}{(\Delta x)^2}(T_{m+1,n} + T_{m-1,n} - 2T_{m,n})$$

$$\frac{\partial^2 T}{\partial y^2} \approx \frac{1}{(\Delta y)^2}(T_{m,n+1} + T_{m,n-1} - 2T_{m,n})$$

By substituting the approximations in the heat equation we arrive at:

$$\frac{1}{(\Delta y)^2}(T_{m,n+1} + T_{m,n-1} - 2T_{m,n}) + \frac{1}{(\Delta x)^2}(T_{m+1,n} + T_{m-1,n} - 2T_{m,n}) + \frac{1}{k}\frac{\partial q}{\partial t} = 0$$

where heat generation in the element is included by adding the term $\frac{1}{k}\frac{\partial q}{\partial t}$. With the help of computers, this meshing reduces the complexity of the solution drastically allowing us to solve more complex geometries. The FEM is accordingly extrapolated to three dimensions with varying element sizes of varying shapes. In the simulations carried out in the current thesis, tetrahedral element geometries were used for all objects.

3.1.1 Wheel Mesh Example

For the simulations executed for the current work, a tetrahedral mesh of 3mm lengths was used for the wheel geometry. An example view of such mesh is shown in figure 3.2.

3.2 Loads, Constraints and Physical Simulations

Within the NX FEM software used in the current work, multiple methods exist to simulate most physical phenomena. A comparison between different models available in the software was performed in the preliminary analysis of every studied case and the model with the most realistic results, based on theoretical interpretations, was chosen. In this section, an overview of the models is given, as well as how each one incorporates the relevant theoretical representation.

3.2.1 Radiative Heating

To simulate the radiative heating of the target wheel due to the incident particle beam, the beam dimensions and impact spot must be well known. These beam parameters vary significantly according to the type of experiment executed at the facility and the desired extraction method. In most cases, a circle of 3mm diameter is chosen to represent the beam impact spot.

This incident radiation is modelled using calculations of radiative heating. In addition to the existing geometry, a cylinder of the circular dimensions of the beam is modelled into the system and placed at a distance away from the beam impact point such as in figure 3.3. This is done such that a radiative heating model can be used, with the cylinder as the emitting region and the wheel as the absorbing surface. Fittingly, the incident power can then be specified and is supplied as 4 kW. Adding such an external cylinder to the system not only allows the implementation of radiative heating but also allows for including motion of the wheel with respect to the beam spot.

3.2.2 Thermal Loads

An alternative to the aforementioned method of applying radiative heating would be to simulate the incident radiation as a heat load across a specified volume. In contrast to radiative heating, the thermal loads model applies the power equally to a specific chosen volume, as opposed to a surface. This allows for better modelling of the penetrative behaviour of the incident particle beam. The thermal load can also be adjusted to

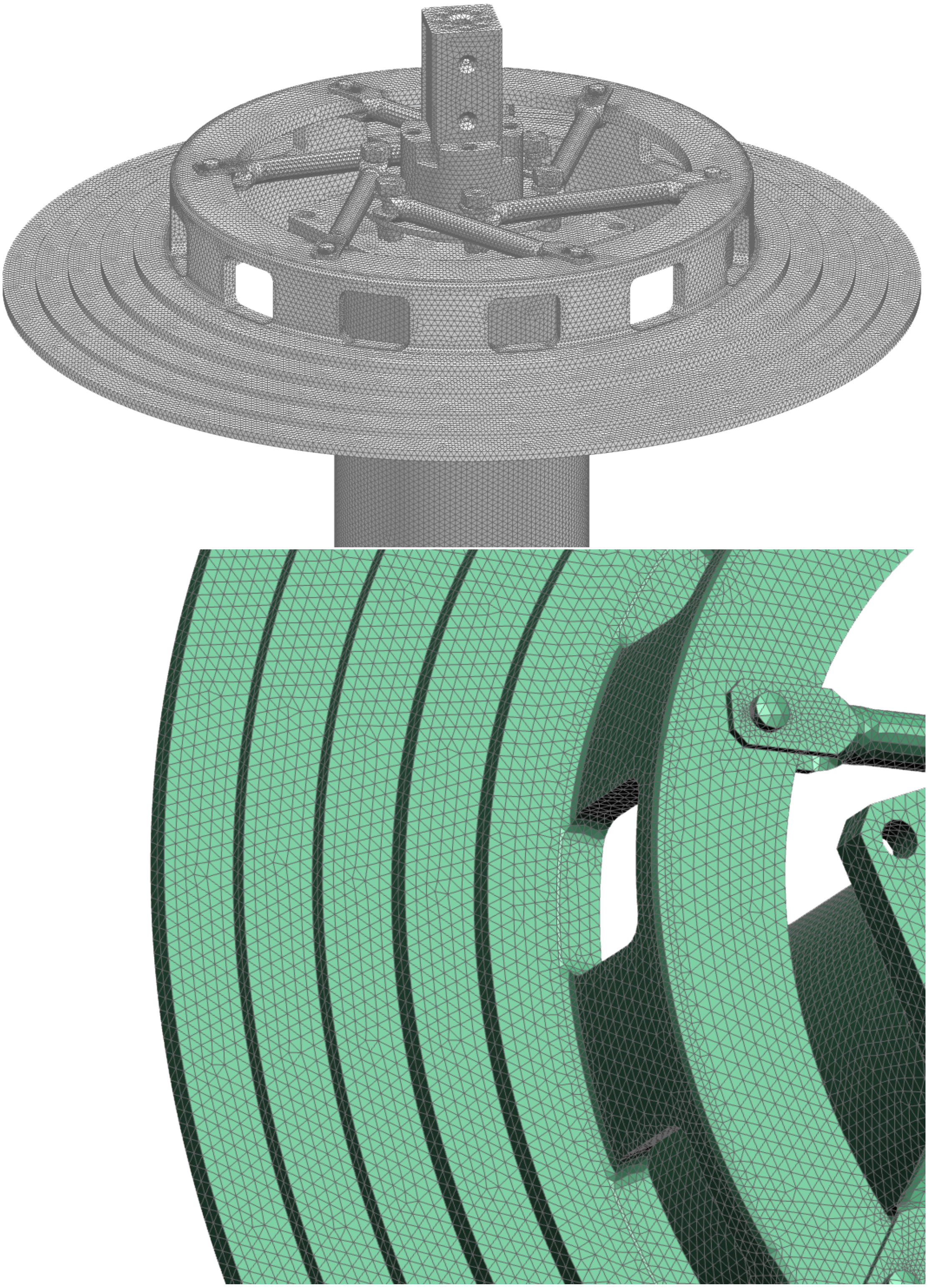

FIGURE 3.2: Example of the wheel's 3mm tetrahedral mesh

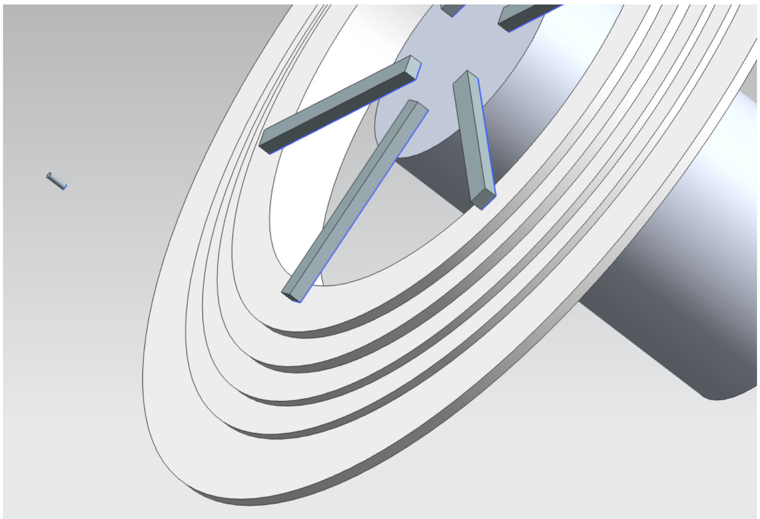

FIGURE 3.3: Setup for the simulation of radiative heating using an additional cylinder

simulate a heat flux on a surface, which supports the simplification of a rotating wheel model discussed later.

3.2.3 Articulation

Since the design choice of a target wheel is such to increase the interaction volume and reduce target damage by rotating the wheel, the rotation must be correctly modelled in the current analysis. The rotation of the wheel is done by implementing an articulation rotation of the wheel around its central axis, which coincides with the central axis of the motor. The wheel rotates at 1 revolution per second with a specified 200 steps per rotation as detailed in the specifications of the motor [11].

Considering that the implementation of the articulation drastically increases the computation time, the behaviour of the beam spot and the residual heat (beam tail) will be studied with a rotating wheel and then reduced to a simplified thermal model. This simplified simulation will model the heat load of the incident beam as a function which describes the thermal results obtained from the implementation of the articulation. Thus, by using the Thermal Loads module for heat flux, the computation time can be reduced for more advanced calculations while maintaining the physical realism of the thermal calculations.

3.2.4 Heat Transfer

In the studied system, heat transfer occurs through conduction and radiation only. These mechanisms are modelled by implementing various modules within NX. In simulations where the chamber walls are not included, radiation to environment is included and the objects then radiate their heat to an object infinitely away. Additionally, perfect contact between dissimilar meshes must be defined, otherwise the solver will not account for conduction although the objects could be touching.

There exist several ways to simulate radiative heat transfer. For simulations of a simplified target wheel (i.e. excluding its surroundings) a simple radiation to environment model is implemented. In the radiation to environment model, the effective emissivity (emissivity$\times$GBVF) of the objects have to be defined. Alternatively, a Monte Carlo method is used in simulations where the radiation between objects and their surroundings have to be accurately calculated, such as simulations concerning the entire target station. In such simulations, there is no radiation to environment within the station's radiation enclosure. The Monte Carlo method generates a number of rays per element at random directions. The rays are then traced until extinction and accordingly the GBVFs between the emitting and receiving elements are calculated.

3.2.5 Flow Boundary Conditions

In order to implement the designed cooling systems, fluid flow parameters for the water based cooling must be actualised. First, the fluid geometry must be specified and in the current study it is assumed the water fills the pipes and channels of the cooling system. Once the geometry is implemented, the water flow boundary conditions are added to the solver. For each independent cooling supply, the water flow direction is specified by an inlet and an opening. Finally, the volumetric flow speed of the water is defined.

For the cooling system implemented in the current work there exists many pipes and passages which are narrow enough to induce turbulent flow at the used volumetric speeds. In the current analysis, all flow conditions will be solved using an adaptable solver. The flow module analyses the flow geometries and calls on different solvers depending on the calculated Reynolds numbers. In most cases considered, turbulent flow is present and is solved numerically using the K-Epsilon method [12].

3.3 Solutions

The solutions in the Siemens NX program utilise multiple physics modules compiled together in the thermal/flow environment. These modules independently calculate multiple parameters ranging from element connections to grey body matrices. The method and order in which these modules are called depend primarily on the type of solution:

steady state or transient solutions. This section will explain the two solver mechanisms and give insight into when each is employed.

3.3.1 Steady State Solutions

Steady state solutions, also known as equilibrium solutions, imply that the parameters of the solutions are independent of time. In the thermal/flow context this implies that the calculation is done such that the temperature gradients in the bodies are constant. This follows from the heat transfer Laplace equation:

$$k(\frac{\partial^2 T}{\partial x^2} + \frac{\partial^2 T}{\partial y^2}) = \rho C \frac{\partial T}{\partial t}$$

with $\frac{\partial T}{\partial t} = 0$.

Such steady state solutions are used in cases where the heat loads applied are constant and result in a consistent temperature gradient throughout. Since the steady state calculation does not take into account temporal factors and motion into account, the solutions generally compute much faster, decreasing the computation time significantly.

3.3.2 Transient Solution

In cases where the motion of the objects is to be considered, transient solutions, also known as time dependent solutions are applied. Transient solutions output the required results for thermal and flow analysis at detailed time steps. The solution starts at the specified initial conditions and computes the characteristics of the system at defined time intervals based on the results of the last time step. Such solutions are then much more accurate since no equilibrium conditions are assumed. The length of the time step is a user specified parameter which can affect the results considerably. If the system exhibits fast changes but the time step is long, the effects will be averaged and in most cases not representative of the physical situation. Accordingly, the time step value chosen must be as small as possible while taking into account the increased computation time. In the current work, the time step for major transient solution is reduced until convergence of temperatures is obtained.

Chapter 4

Results

In this chapter, the results of the executed thermal and flow simulations are presented. Additionally, investigations of the effects of varying the input parameters are given. A bottom-up method was used, as the simulations were incremented in complexity, increasingly representative of the physical situation. The first section of the results lays out the simulations for the isolated target wheel as a simplified model. First, an incident heat load of 4 kW impacts a stationary isolated target wheel. Next, the rotation of the target wheel is implemented and a comparison to the stationary analysis is given. Furthermore, the geometries of the motor and the spokes are added and the heat propagation to the motor and its steady state temperatures are analysed. Subsequently, the cooling systems are added and the water flow is considered. Finally, the results of the preliminary simulations are implemented into a complete model of the target station and the detectors' temperatures are given.

4.1 Reduced Target Wheel

In this section, thermal analysis is executed to determine the steady state temperatures of an isolated target wheel. The simulations are preliminary and were designed to investigate the physics of the interactions and heating of the wheel as well as to give motivation for the implementation of a cooling system.

4.1.1 Stationary

As shown in figure 4.1, an isolated wheel is meshed at 2.5mm and a heat load of 4 kW is applied to a cylinder within the wheel of dimensions identical to the beam dimensions (3mm). A stationary wheel with no thermal constraints will heat up indefinitely thus

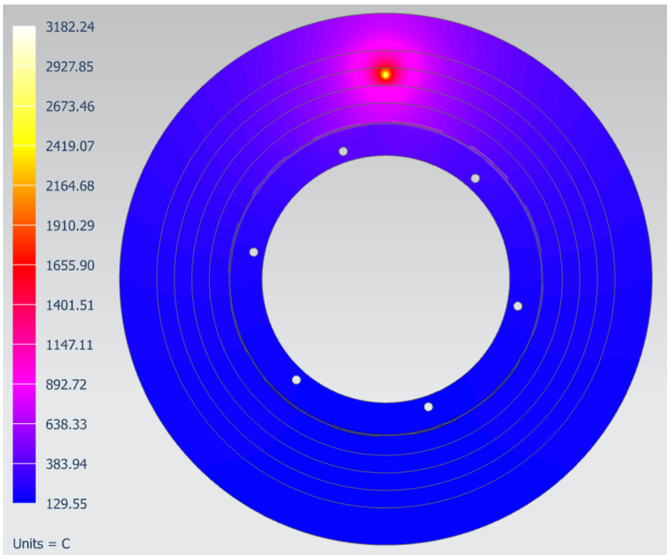

FIGURE 4.1: Thermal profile of isolated stationary target wheel

a radiation constraint was added to the reduced target wheel. The thermal results for steady state computation are shown in figure 4.1. The target wheel reaches temperatures of about 3182° which are well above the phase transition limits of the selected material.

4.1.2 Integration of Articulation

4.1.2.1 Complete wheel

In this subsection the motion of the wheel is modelled using articulation modules. The wheel is set to rotate at 1 revolution per second. The radiative heating model is used, where the emitting region is a cylinder with a radius of the width of the beam: 3mm. The transient solution was computed for two seconds and a sample of the results at an intermediate time step are shown in figure 4.2. Since the solution for two rotations executed in 5.5 days, to analyse thermal profile for longer periods of time, the model had to be further reduced.

4.1.2.2 Arc Reduced

An arc cutout of the wheel as shown in figure 4.3 is studied using transient solutions for several seconds. A similar radiative heating mechanism is used as for the complete wheel. Two beam dimensions of 6mm and 1mm $\times$ 2mm where used and the corresponding temperature results are shown in figure 4.3. It can be seen that in the case of a smaller beam size, the individual heat spots due to discretised rotational calculations

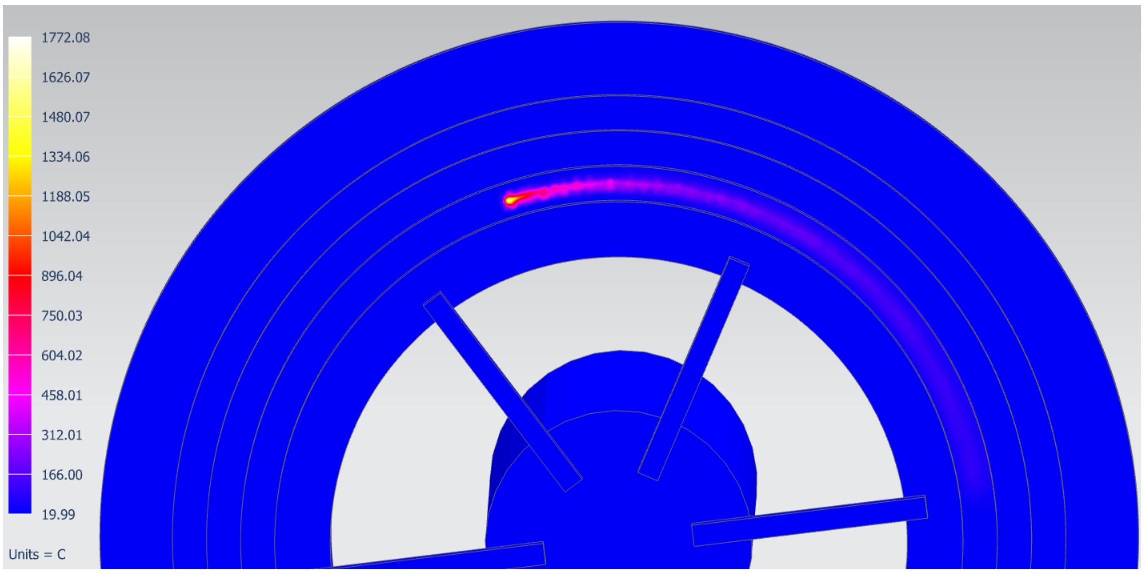

FIGURE 4.2: Transient solution for a simplified model with a circular beam spot of 3mm

are separated. However, for 6mm, the beam size is larger than the stepper motor resolution, thus no individual spots are seen. Furthermore, to characterise the beam tail on the wheel such that it could be modelled in prospective steady state analyses, the temperature evolution of locations on the beam tail are inspected and shown in figure 4.4.

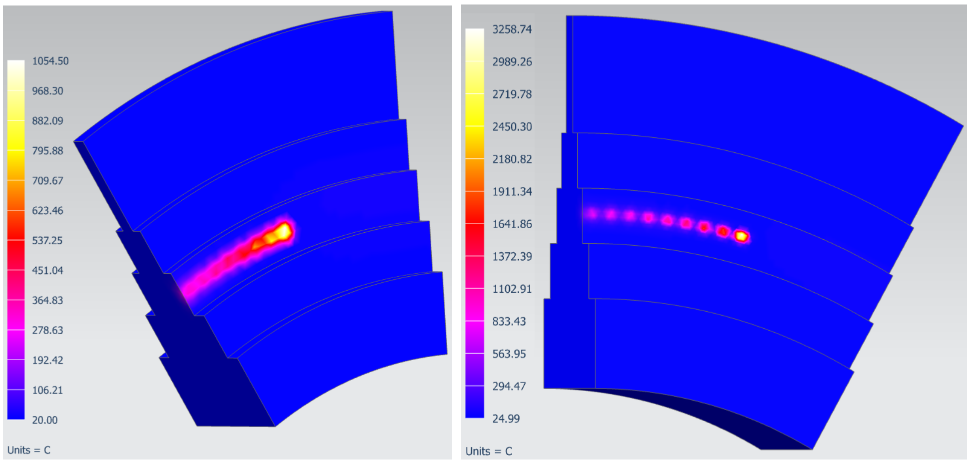

FIGURE 4.3: Arc cutout of the wheel for transient analysis of the beam spot and tail shape. 6mm and 1mm × 2mm for left and right,respectively

4.2 Motorised Target Wheel

Data from the transient analysis illustrated before is used to describe a heat load function. The heat load function should be a simple function which characterises the shape

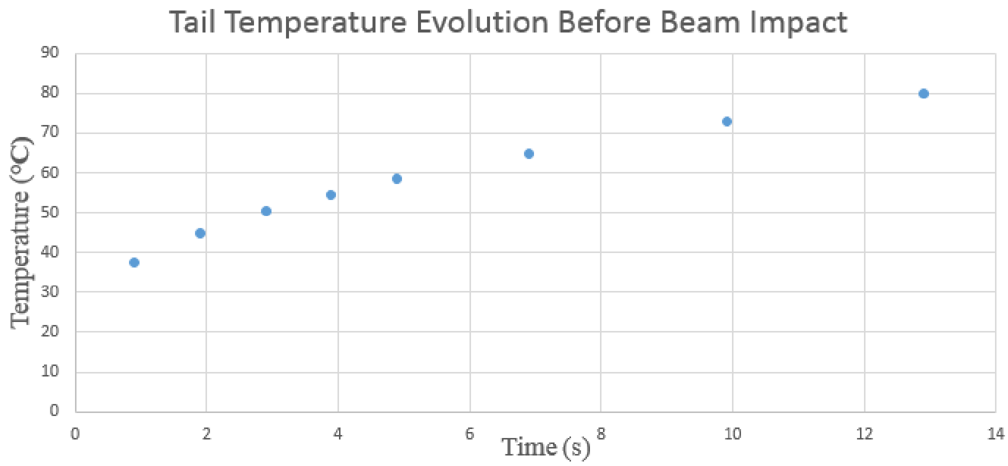

FIGURE 4.4: A plot of the converging beam residual temperatures at 0.1 seconds before beam impact

of the beam and residual heat (beam tail) as accurately as possible. For the purposes of this study, a simple Gaussian function is used. For the function to be implemented, the flux, ϕ, must be a function of θ, the angle around the wheel with $\theta = 0$ at the beam impact spot. The integral of the Gaussian function over the beam size is set to be equal to the total thermal load applied by the beam, 4 kW. Accordingly, the coefficients are determined and the heat flux is imposed as:

$$\phi = 25e^{-\frac{1}{2}(\frac{\theta}{5})^2}$$

This function is then used as the thermal load for all consequent steady state analyses. The wheel spokes and the motor are added to the model and a steady state analysis with the heat flux as specified is calculated. Results are as shown in figure 4.5. Motor temperatures reach $100°C$ at the spokes' contact. The motor bearing reaches $50°C$ excluding the heat generated due to friction at that point. At these temperatures, the motor is expected to fail according to its specifications [11], thus adding to the need for a cooling system.

4.3 Water Cooling System

Before the cooling system can be implemented into the model, independent flow analysis need be performed to ensure no water blockages and most importantly test the physical validity of the laminar/turbulent flow solutions for the designed fluid conveyance. This analysis is done independently for the front and back plates. The motor cooler plate has not been accurately designed yet and currently the model hosts regular pipes eliminating the need for flow analysis.

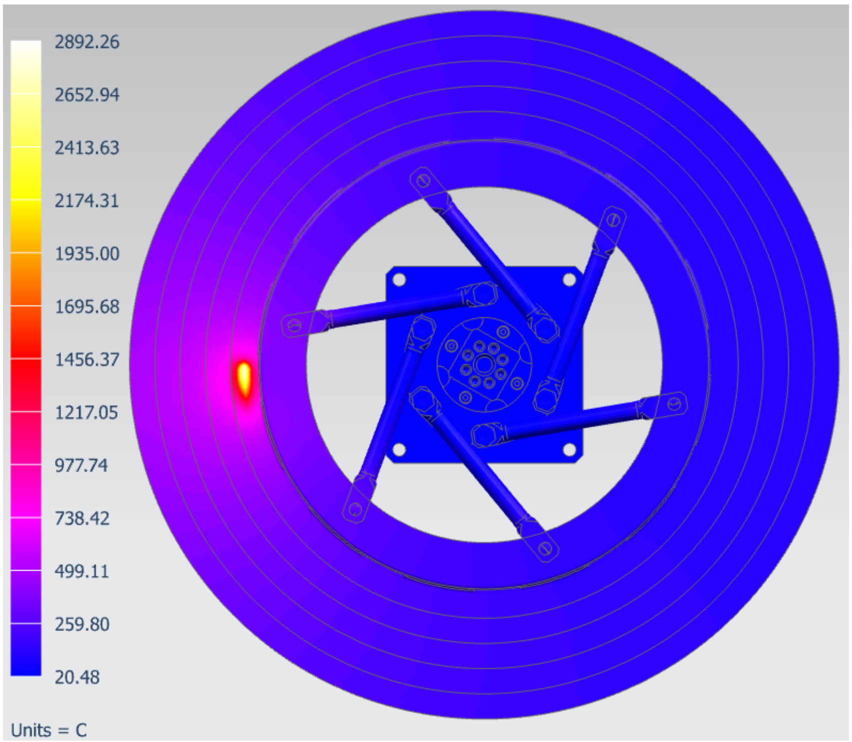

FIGURE 4.5: Thermal results of the simulated beam thermal profile using a Gaussian function.

4.3.1 Front Plate

The K-epsilon turbulence solver including wall friction has been used for the following fluid analyses. In figure 4.6 the resulting steady state water pressure increase and velocities are shown. From the velocity profile it is observed that there are multiple locations at which there is constricted water flow. These occur at the corners of the conveyance and are named flow 'dead spots'. Although water has a high heat capacity, dead spots are unfavourable in cooling systems as there is a possibility of phase transition of the trapped water. This will result in relatively high pressure spikes which affect the flow of the entire cooling loop.

The pressure profile of the front plate shows safe pressure levels well below 20,000 Pa above inlet pressures. Since the mechanism of production of these plates is pressurising the vessels, the plates can withstand values well above the range of the currently calculated pressures.

4.3.2 Back Plate

Similar simulations were run for the back plate and the results for pressure variation and water velocities are shown in figure 4.7. In the back plate there exists multiple water

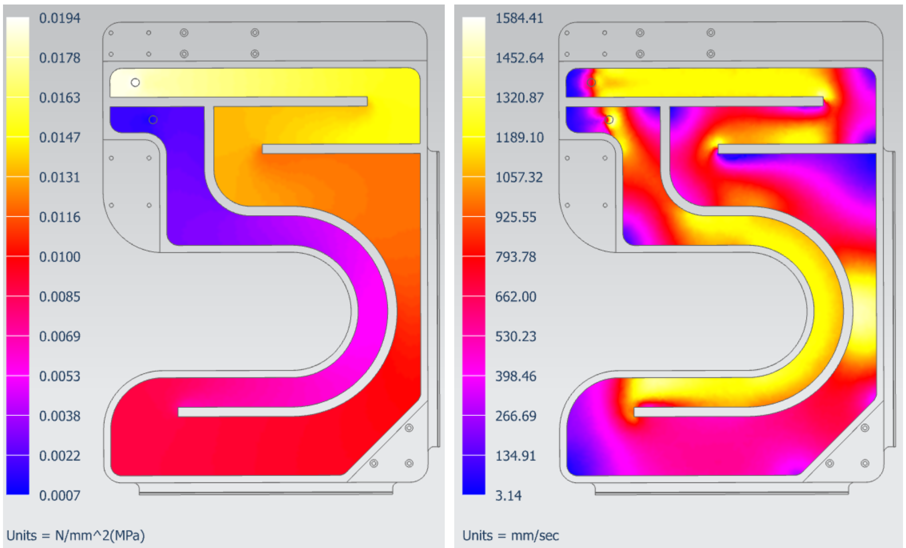

FIGURE 4.6: Pressure variation (left) and water flow velocity (right) in the blown steel front plate.

dead spots as present in the front plate. Similarly, the dead spots manifest at the corners of the conveyance. There are observed lower order pressure variations as compared to the front plate. This is due to the back plate's wider channels and the lack of locations where the flow is constricted.

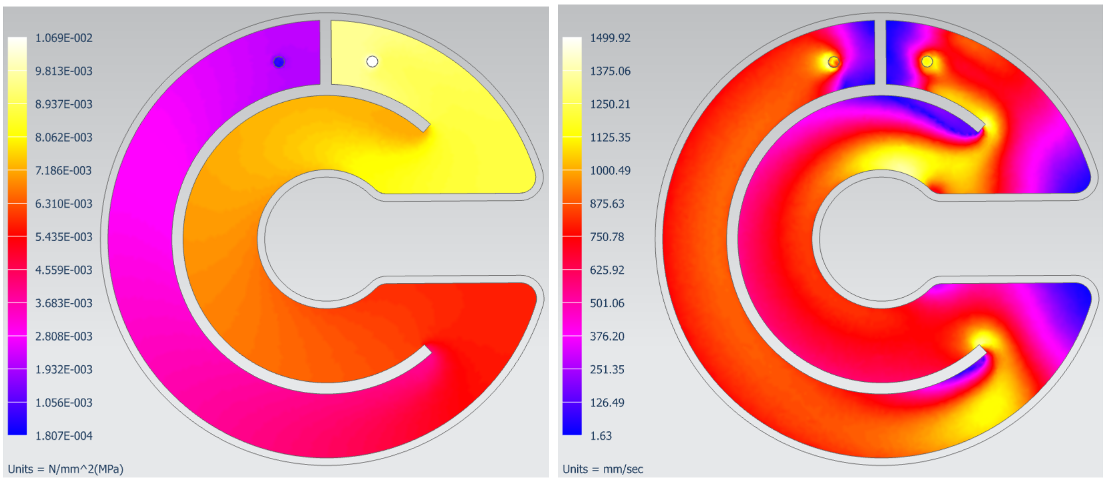

FIGURE 4.7: Pressure variation (left) and water flow velocity (right) in the blown steel back plate.

Accordingly, the cooling system is added to the wheel and motor geometries and thermal/flow simulations were run. The resulting temperature profile is shown in figure 4.8. The water is found to exit at $27.4°C$ extracting 1173 W of power. The motor temperatures do not exceed $50°C$ with the highest temperature $49.4°C$ found at contact with the spokes. The bearing temperatures reach $31°C$, indicating a temperature rise of $11°C$, in addition to the temperature rise induced by friction.

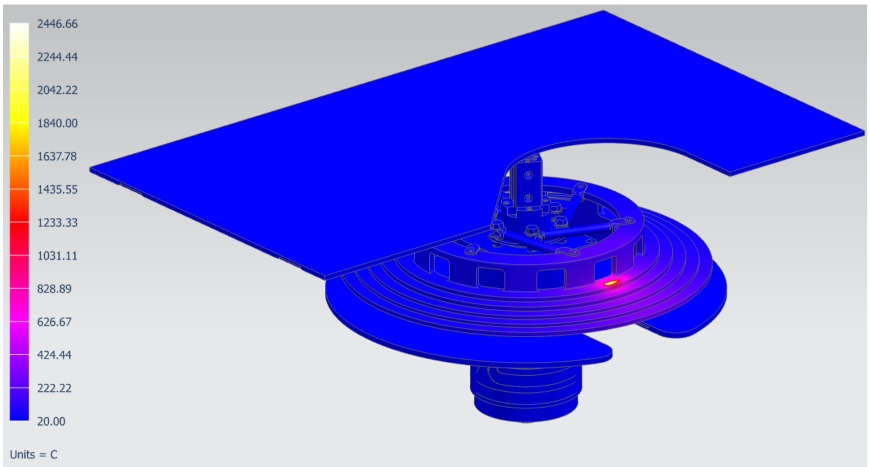

FIGURE 4.8: The temperature profile of the system when the cooling system is applied

To provide clear contrast between before and after the implementation of the cooling system as well as to demonstrate its effectiveness, the motor temperatures with and without the cooling system are shown in figure 4.9.

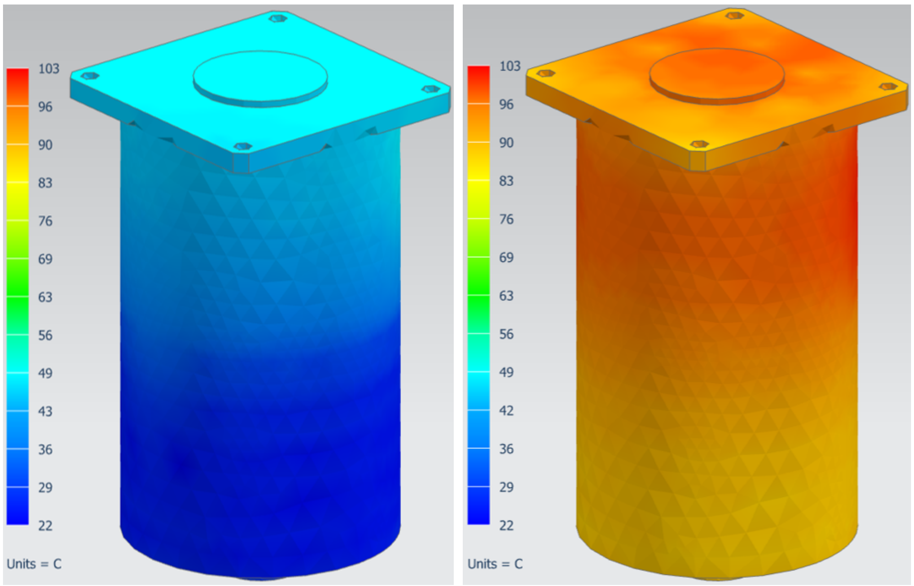

FIGURE 4.9: The motor temperature profile with (left) and without (right) the cooling system

4.4 Target Station

This section works on extending the scope of the current simulations to include the target station as a whole. These simulations use results of the previous detailed simulations such that the computation time is reduced. The aim of integrating the chamber and the station is to ensure the detectors and apparatuses in adjacent chambers are safe from the radiated thermal energy and could therefore operate ordinarily.

The radiation between components in the target station analysis was not specified by the author. Instead the Monte Carlo rendering method was used to calculate the GBVFs at 200 rays/element. This ensures correct modelling of the radiation within the station enclosure, which is the main mechanism of energy transfer, since the station is held at vacuum.

The simulation is executed without a cooling system and the steady state results are shown in figure 4.10. The beam diagnostics detectors reach temperatures of $212.2°C$, $149.0°C$ and $129.5°C$, respectively away from the wheel.

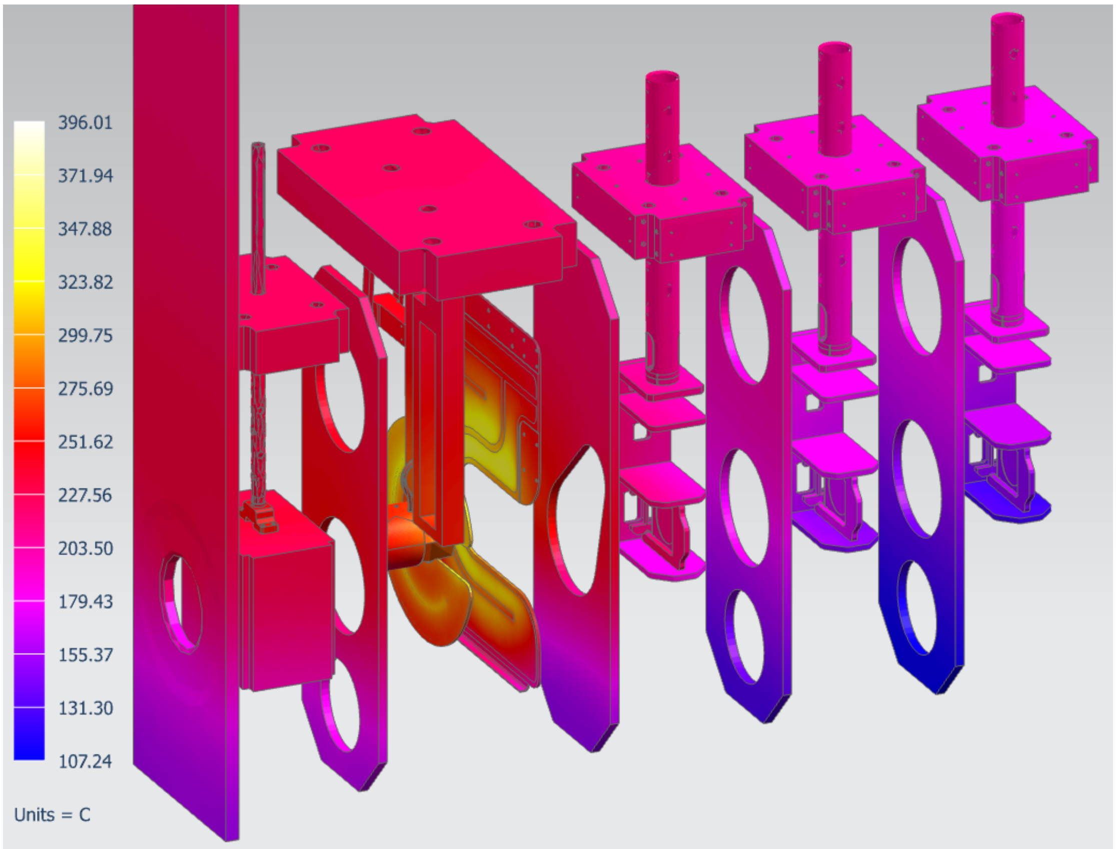

FIGURE 4.10: Thermal results of the target station with no cooling system. The figure excludes temperatures of the wheel and the station's external walls.

The cooling system including pipes is then added to the model and GBVF between the target station's 542,898 elements are set to be recalculated. There are 57,283,400 view factors calculated using a Monte-Carlo method with 200 rays calculated per element. In this simulation, 500 W have been applied on the collimator inner geometry as this is the expected power generation at that location according to the SFRS documentation [8]. The resulting temperature profile is shown in figure 4.11. With cooling implemented, the detectors reach temperatures of $157.3°C$, $100.2°C$ and $84.6°C$, respectively away from the wheel. Water temperatures through the outlet reach $28.8°C$ which implies the cooling system extracts 1856W of power from the station.

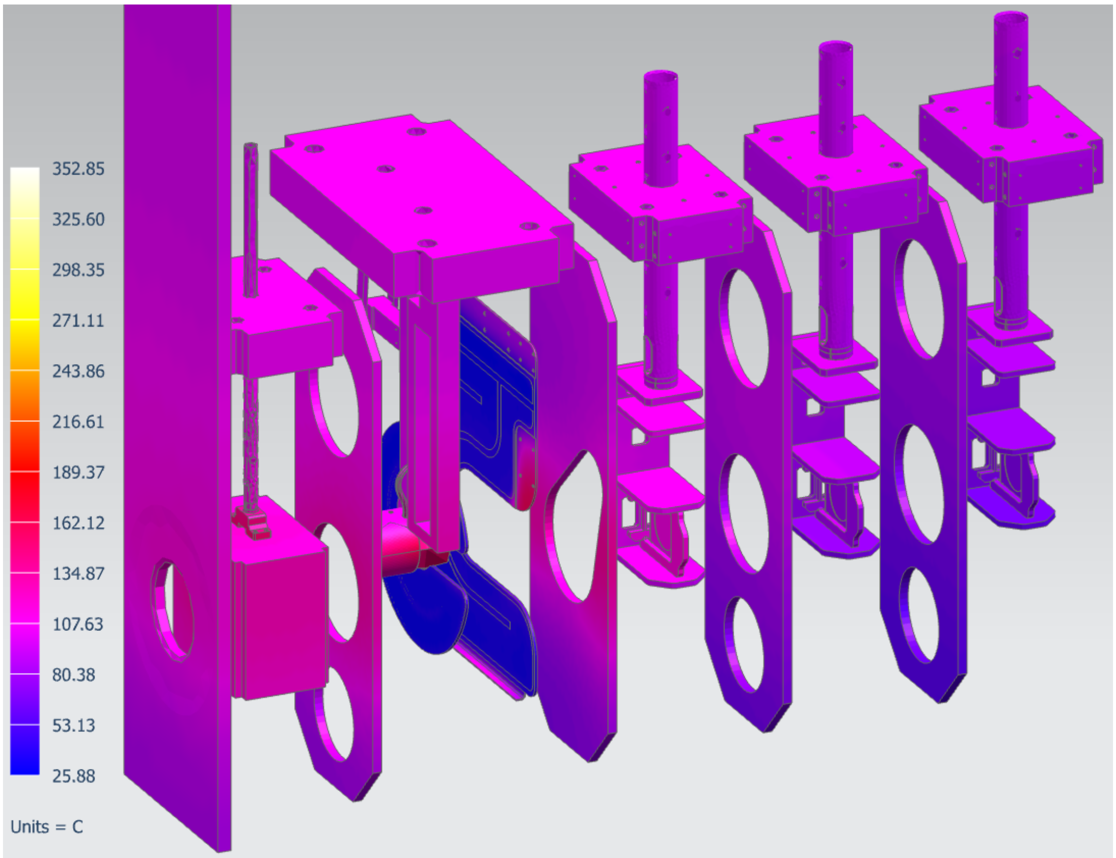

FIGURE 4.11: Thermal results of the target station with the cooling system. The figure excludes temperatures of the wheel and the station's external walls.

4.5 Mesh Sensitivity Analysis

In the simulation results presented so far, varying mesh sizes for the geometries studied were used. In choosing the mesh size for the selected geometries, several factors have to be taken into account: mesh quality, physical realism and expected computation time. Mesh quality refers to consistency of the mesh throughout the volume, curvature sensitivity and parameters concerning the local element-element connections. Physical realism is inferred through the mesh size and the variation of mesh sizes throughout the volume. The realism of the mesh depends on the solution considered. For smaller meshes, the solutions tend to be more realistic and representative of the scenario considered. Finally, the expected computation time influences the decisions, since as demonstrated, some solutions are expected to take months in computation. The computation time increases with increasing element count (i.e. decreasing element size). A suitable balance between computation time and element size is to be found for vital complex geometries.

The simulation software NX provides an analysis tool to assess the mesh quality. The mesh sensitivity analysis provided operates on a pre-defined solution. The analysis then computes the solution repeatedly while decreasing the element size with each repetition.

This is carried out until the local change in the calculated temperature is lower than a predefined limit, thus a converging solution. Accordingly, a final mesh is provided which is assumed to be physically accurate for the analysed solution chosen. This method of mesh sensitivity analysis operates on tetrahedral 3D meshes only and is used for simplified solutions. The resulting meshes were then studied and their data was used to infer better mesh sizes for more complicated solutions.

Chapter 5

Discussion

The present study was designed to determine the effect of ion beam irradiation on the target station at FAIR. The main objective was to assess the temperatures at the critical points in the station and to implement a water cooling system. The critical points in the station were identified to be the beam interaction point, the motor and the detectors. The temperatures at these locations were studied with and without the implementation of a cooling system and the results are presented in detail in chapter 4.

The current study found that the motor temperatures in the system reach $100°C$ at the contact with the spokes at steady state without water cooling. These temperatures are too high for the motor to operate normally and under such conditions, it is expected to fail. Additionally, the motor bearing was found to reach temperatures of $50°C$ excluding the temperature resulting from friction. It is then predicted that this $30°C$ increase in the temperature will add to the temperature increase due to friction and result in higher temperature than the one presented in this work. Again, such temperatures hinder the performance of the motor and limit its operational lifetime.

With the implementation of a cooling system designed and modelled by B. Eng. M.F. Lindemulder, the motor temperatures are observed to drastically decrease. With such a cooling system run at 7 l/min volumetric water flow, the motor temperatures do no exceed $50°C$ and the bearing temperature increases by up to $11°C$ above initial temperatures. It can then be concluded that the implementation of a water cooling system ensures normal operating temperatures for the motor.

Another important finding was that the detectors closest to the wheel reach temperatures of about $212°C$. This temperature is higher than the recommended temperatures for any of the detectors designed to be added to the detector ladders considering the electronics present. The two detectors further from the wheel reach temperatures of about 149 and 130°C. The relatively high temperature of the first detector is attributed to the proximity of the detector to the target wheel as well as the detector is un-shielded from beam spot. For the latter two detectors, the temperature is due to proximity as well as enclosure reflectivity. These temperatures imply a requirement for the implementation of a cooling system.

The detector temperatures are show to reach lower temperatures with the implementation of the cooling system. In order away from the wheel, the detectors have temperatures of 158°C, 101°C and 85°C. These temperatures do not allow for orderly operation of the detectors. In operation however, the detectors are not placed within the beam direction at high beam intensities and energies. Since the detectors are beam diagnostic detectors, they are only operated at low beam intensities which implies a lower heat load than the one imposed in the current simulations. This will result in much lower steady state temperatures of the detectors. All simulations including the detectors assume they are grey bodies with emissivities similar to steel, as most exposed components are. Additionally, it is assumed no heat is produced within the detectors themselves due to beam interaction. Future studies on the current topic are therefore recommended to study the thermal properties of the detector chambers in more detail.

It is calculated that the power extracted by the water is 1857kW which removes 46.4% of the heat produced in the wheel. This extracted power calculation is based on the outlet temperatures of the water in the cooling system and the flow parameters. Alternatively, the heat conducted to the water could be retrieved through the flow solver in NX. However, it was observed the values in the power conducted fluctuate significantly and in most cases overshooting the input power. Thus, only calculated values based on the water temperatures were presented.

There are several adjustments which can be made to ensure lower temperatures than the ones calculated here. By increasing the wheel's rotation speed from the current 60rpm to 180rpm, which is supported by the motor [11], the interaction volume increases. However, such high rotation speeds might result in structural instabilities particularly at higher temperatures. Higher speeds will only result in lower temperatures if the spill frequency of the particle beam is adjusted accordingly. Furthermore, adjustments to the cooling system can be made to increase its efficiency. Faster water flow or lower initial water temperatures are an example of such viable adjustments.

In order to conserve simulation run-time, the transient solutions were used to simplify the beam characteristics for use in steady state analyses. The beam spot and tail were reduced to a Gaussian function with fitted parameters to the transient solution. However, one major drawback of using steady state solutions is the steady input load at the beam spot because the heat load is applied to the same location since there is no rotation. This results in higher beam spots temperatures as shown in the results, section 4.2. Consequently, there is more radiated heat to the environment including the motor, cooling system and detectors. Thus, the steady state solutions presented in the current work are taken to be representatives of worst case scenarios. The beam heat load has been continuously modified to result in temperatures similar to the transient solutions while maintaining correct power loads.

The simplified beam heat load was applied to the wheel geometry using a heat flux module. The module requires specifying a surface onto which the heat load is applied. Accordingly, the simplified beam heat load was applied on a small surfaces of width 3mm facing the beam. This implies the beam does not penetrate into the wheel in these calculations which is not representative of the real situation. An alternative solution would be to apply the simplified beam as a heat load over the target thickness equally. Attempts have been made to implement such a solution but heat loads throughout the volume do not support complex functions as input, and thus the Gaussian function could not be implemented.

It is assumed throughout this study that the properties of materials are independent of temperature. This assumption is not valid specifically in the case of surface emissivity. The value of emissivity changes by up to 15% within the temperature ranges reached within this study. This change will in turn affect the total radiated energies and might result in different operating temperatures for the motor and the detectors. Accordingly, in cases where the value of emissivity and its temperature dependence are unknown, worst case scenarios were considered. For example, in scenarios where the temperature of the motor is studied, a higher value of emissivity for the wheel's graphite is used. Further experimental work is required to determine the emissivity of the target wheel and its temperature dependence.

Values and results presented in the current work do not show the uncertainties in the values. This is due to the fact that simulations are deterministic and the uncertainties in the calculated values could only be guessed, or otherwise inferred by comparing them to experimental data, which are not available for this study. Uncertainties in the calculated values could also not be inferred through the comparison of identical runs, as the runs result in the exact same values. Conversely, the error in the temperatures could be calculated by applying different meshes to the geometries and deduce the mesh-result dependency. For the executed simulations presented here, mesh sensitivity analyses have been performed and the convergence meshes were used for simulations of the stated results. A suggestion for future work would be to assess the physical validity of the thermal/flow modules used through the aid of experimental studies at the current fragment separator facility [8].

Chapter 6

Conclusion

The aim of the present research was to examine the effects of ion beam irradiation on the graphite target wheel at FAIR. Additionally, a cooling system design, designed by B. Eng. M.F. Lindemulder, for the target wheel assembly has been implemented and tested using FEM thermal/flow simulations. It has been determined the cooling system is sufficient at cooling the target wheel and the motor such that they operate at recommended temperatures. However, it is observed that the beam diagnostics detectors reach high temperatures which can hinder their performance or disable the electronics.

The current data highlight the importance of the implementation of the cooling system, without which the motor temperatures rise above $100°C$ which limits the lifetime and performance of the motor. With the cooling system implemented, the motor temperatures do not exceed $50°C$. This ensures normal operation of the motor. The findings of this investigation complement those of earlier experimental studies performed on similar target wheels [13][14].

A limitation of this study is that it does not simulate the structural deformations of the target wheel. Similarly, affected values are not considered such as the change in emissivity due to surface etching. Being limited to FEM simulations, this study lacks experimental proofing of the calculated values. This would be a fruitful area for further work as demonstrated in the studies by W. Mittig [14]. Finally, further work needs to be done to establish whether the temperatures of the detectors as calculated in the current study are realistic and if the radiation calculations are limited by the Monte Carlo simulations.

Bibliography

[1] APPA. APPA Physics. *Online Access*, 2018. URL https://fair-center.eu/for-users/experiments/appa.html.

[2] APPA. APPA Research at GSI. *Online Access*, 2018. URL https://www.gsi.de/en/work/research/appamml.htm.

[3] CBM. The Compressed Baryonic Matter (CBM) experiment . *Online Access*, 2018. URL https://fair-center.eu/for-users/experiments/cbm.html.

[4] PANDA. Panda collaboration. *Online Access*, 2018. URL https://panda.gsi.de.

[5] H. Geissel and H. Weick et al. The Super-FRS project at GSI. *Nuclear Instruments and Methods in Physics Research Section B: Beam Interactions with Materials and Atoms*, 204:71 – 85, 2003. ISSN 0168-583X. doi: https://doi.org/10.1016/S0168-583X(02)01893-1. URL http://www.sciencedirect.com/science/article/pii/S0168583X02018931. 14th International Conference on Electromagnetic Isotope Separators and Techniques Related to their Applications.

[6] Super-FRS Collaboration. Scientific program of the Super-FRS collaboration : report of the collaboration to the FAIR management. Technical Report GSI Report 2014-4, Darmstadt, 2014. URL http://repository.gsi.de/record/67533.

[7] J. Aysto and K.-H. Behr et al. Experimental Program of the Super-FRS Collaboration at FAIR and Developments of Related Instrumentation. *Nuclear Instruments and Methods in Physics Research Section B: Beam Interactions with Materials and Atoms*, 376:111 – 115, 2016. ISSN 0168-583X. doi: https://doi.org/10.1016/j.nimb.2016.02.042. URL http://www.sciencedirect.com/science/article/pii/S0168583X16001725. Proceedings of the XVIIth International Conference on Electromagnetic Isotope Separators and Related Topics (EMIS2015), Grand Rapids, MI, U.S.A., 11-15 May 2015.

[8] H. Geissel et al. Technical Design Report on the Super-FRS. *FAIR Technical Document*, page 143, December 2008.

[9] N.V. Mokhov and F. Cerutti. Beammaterial interactions. *CERN Yellow Reports*, 2(0):83, 2016. URL https://e-publishing.cern.ch/index.php/CYR/article/view/231.

[10] J.P. Holman. *Heat transfer*. Mechanical engineering series. McGraw-Hill, 1989. ISBN 9780071004879.

[11] Phytron. VSS / VSH Stepper Motor: For Applications up to Ultra-high-vacuum. *Technical data sheet*, 4 2017. URL www.phytron.eu/vss-vsh.

[12] J.E. Bardina. *Turbulence Modeling Validation, Testing, and Development*. NASA technical memorandum. National Aeronautics and Space Administration, Ames Research Center, 1997. URL https://books.google.nl/books?id=qKM3AQAAMAAJ.

[13] Sabine Riemann, Felix Dietrich, Gudrid Moortgat-Pick, Peter Sievers, and Andriy Ushakov. The ILC Positron Target Cooled by Thermal Radiation. In *International Workshop on Future Linear Collider (LCWS2017) Strasbourg, France, October 23-27, 2017*, 2018. URL https://inspirehep.net/record/1651525/files/arXiv:1801.10565.pdf.

[14] W. Mittig. The FRIB High Power Production Target Development. *FRIB*, 5 2011. URL http://www.hep.princeton.edu/mumu/target/Mittig/Mittig_050311.pdf.